CONDITIONING ANALYSIS OF NONLOCAL INTEGRAL OPERATORS IN FRACTIONAL SOBOLEV SPACES

BURAK AKSOYLU* AND ZUHAL UNLU†

December 19, 2013

Abstract. We study the conditioning of nonlocal integral operators with singular and integrable kernels in fractional Sobolev spaces. These operators are used, for instance, in peridynamics formulation and nonlocal diffusion. In 1D, we present sharp quantification of the extremal eigenvalues in all three parameters: size of nonlocality, mesh size, and regularity of the fractional Sobolev space. We accomplish sharpness both rigorously and numerically.

For the minimal eigenvalue, we obtain sharpness analytically by using a nonlocal characterization of Sobolev spaces. We verify this estimate by exploiting the Toeplitz property of the stiffness matrix. However, the analytical approach fails to give sharp quantification of the maximal eigenvalue. Hence, in 1D, we take an algebraic approach by directly working with the stiffness matrix entries, which have complicated expressions due to all three parameters. We systematically characterize the nonzero entries and dramatically simplify their expressions by using convenient algebra. We establish the zero row sum property of the stiffness matrix and negativity of the off-diagonal entries. Eventually, we arrive at sharpness through the use of the Gerschgorin circle theorem.

Key words. Condition number, nonlocal operators, peridynamics, nonlocal diffusion, Toeplitz matrix, the Gerschgorin circle theorem, preconditioning.

AMS subject classifications. 34B10, 65F35, 45A05.

1. Introduction.

The integral operators under consideration are used, for instance, in peridynamics (PD), a nonlocal extension of continuum mechanics developed by Silling [51], and nonlocal diffusion [5, 14]. The important parameter in these nonlocal formulations is the horizon δ which represents the size of nonlocality. The domain Ω and its nonlocal boundary $\mathcal{B}\Omega$ (a strip of width δ surrounding Ω) define the *nonlocal closure* of Ω:

$$\overline{\overline{\Omega}} := \Omega \cup \mathcal{B}\Omega.$$

We utilize the function space

$$V_D(\overline{\overline{\Omega}}) := \left\{ v \in L^2(\overline{\overline{\Omega}}) : v|_{\mathcal{B}\Omega} = 0 \right\}, \tag{1.1}$$

and $(\cdot,\cdot)$ denotes the L^2-inner product.

We study the conditioning of the weak form of the following nonlocal operator in the fractional Sobolev space $H^s(\overline{\overline{\Omega}})$, $s \in (0,1)$, by assuming $u \in H^s(\overline{\overline{\Omega}})$:

$$\mathcal{L}u(x) = -\frac{2-2s}{\delta^{2-2s}} \int_{\overline{\overline{\Omega}} \cap |x-y| \le \delta} \frac{u(y)-u(x)}{|x-y|^{d+2s}} dy. \tag{1.2}$$

Generalizations of (1.2) in the following form

$$\mathcal{L}u(x) = -c_\delta \int_{\overline{\overline{\Omega}} \cap |x-y| \le \delta} (u(y)-u(x))\gamma(x,y) dy \tag{1.3}$$

*Department of Mathematics, TOBB University of Economics and Technology, Ankara, 06560, Turkey & Department of Mathematics, Louisiana State University, Baton Rouge, LA 70803 USA, baksoylu@etu.edu.tr. This work was supported in part by National Science Foundation DMS 1016190 grant, European Union Marie Curie Career Integration 293978 grant, and Scientific and Technological Research Council of Turkey (TÜBİTAK) TBAG 112T240 and MAG 112M891 grants.

†Department of Mathematics, Louisiana State University, Baton Rouge, LA 70803, USA, zyeter1@math.lsu.edu.

are used in numerous applications such as the modeling of nonlocal diffusion [14, 47], image processing [27], PD [51] and many more. In addition, the fractional Laplacian operator is also an instance of $\mathcal{L}$. See the review articles [14, 37] for a comprehensive discussion and the recent book on PD [38]. We list a few applications in which PD has been effectively used. For instance, in the context of multiscale modeling, PD has been shown to be an upscaling of molecular dynamics [48, 50]. In [6], PD has been demonstrated as a viable multiscale material model for length scales ranging from molecular dynamics to classical elasticity. PD's effectiveness has been established in sophisticated applications such as fracture and failure of composites, nanofiber networks, and polycrystal fracture [42, 52, 53]. In addition, the prediction of crack paths has been successfully modeled by PD [33]. Also see other related engineering applications [11, 32, 34, 43, 44]. We witness an intensive effort to construct mathematical theory [2, 4, 14, 15, 16, 18, 20, 21, 22, 23, 24, 25, 26, 28, 30, 35, 36, 39, 40, 41, 48, 49, 55] and develop numerical methods [1, 3, 12, 17, 19, 46, 54] for PD applications and related nonlocal problems. In this article, we study PD formulations in 1D and nonlocal diffusion in general dimensions. The bilinear forms of interest are given in (1.4) and (1.5).

Studying the nonlocal operator (1.2) in fractional Sobolev spaces is interesting in its own right; see the excellent review article [13]. One of the main reasons that we focus on $\mathcal{L}$ is PD. The fact that PD is an effective model in capturing jump discontinuities in displacement field is a main incentive to study $\mathcal{L}$ in fractional Sobolev spaces. Since such discontinuities arise in the modeling of cracks and failure in the material, it is paramount to study function spaces that contain jump discontinuities. Jump discontinuities belong to fractional Sobolev spaces $H^s(\overline{\overline{\Omega}})$ with $s \in [0, 1/2]$. Unlike the local case, in $H^s(\overline{\overline{\Omega}})$ with $s \in [0, 1/2]$, the trace operator is well-defined and boundary value problems with volume constraints are well-posed [14].

Aside from the horizon δ, the parameters h and s denote the mesh size and regularity of the fractional Sobolev space, respectively. The main goal of this article is to answer the following *open problem: What are the sharp δ-, h-, and s-quantifications in the condition number of the stiffness matrix?* The condition number plays a central role in the development and analysis of preconditioners. Our study lays the foundation of preconditioner research for nonlocal problems in fractional Sobolev spaces. The studies that are most closely related to our results are the first author's preceding work [2, 3] and [14, 55]. The first conditioning results for integrable and singular kernels were reported in [2, 3] and [14, 55], respectively. The corresponding bilinear forms are given in (1.5) and (1.4), respectively. We improve these results by fully revealing sharp δ-, h-, and s-quantifications of extremal eigenvalues, i.e., $\lambda_{\min}$ and $\lambda_{\max}$. We achieve this improvement by resorting to linear algebra, thereby, gaining a big advantage in obtaining sharp quantifications involving all underlying parameters.

For construction of the stiffness matrix, we utilize the weak formulation of (1.2) which gives rise to the corresponding bilinear form [3, Eqn. (3.4)]:

$$a(u,u) = \frac{1-s}{\delta^{2-2s}} \int_{\overline{\overline{\Omega}}} \int_{\overline{\overline{\Omega}} \cap |x-y| \leq \delta} \frac{(u(x)-u(y))^2}{|x-y|^{d+2s}} dy dx. \tag{1.4}$$

We also visit the integrable kernel case with the following bilinear form:

$$b(u,u) = \frac{3}{2\delta^3} \int_{\overline{\overline{\Omega}}} \int_{\overline{\overline{\Omega}} \cap |x-y| \leq \delta} (u(x)-u(y))^2 dy dx. \tag{1.5}$$

The main conditioning results of this article are as follows:

THEOREM 1.1. *For the bilinear forms given in* (1.4) *and* (1.5)*, the following spectral bounds, respectively, provide sharp δ-, h-, and s-quantifications of the extremal eigenvalues for the underlying discretizations:*

$$\underline{c}h \leq \lambda \leq \overline{c}\left(\frac{8(2^{1-2s}-1)}{s(1-2s)(3-2s)}h^{1-2s}\delta^{-(2-2s)} - \frac{8(1-s)}{3s}h\delta^{-2}\right), \tag{1.6}$$

$$\underline{c}h \leq \lambda \leq \overline{c}\left(5h\delta^{-2} - 6h^2\delta^{-3}\right). \tag{1.7}$$

We emphasize that the bounds in (1.6) and (1.7) provide sharp δ-, h-, and s-quantifications of the extremal eigenvalues. In our context, sharpness means that the bounds capture *the exact expression as a function of δ, h, and s* in extremal eigenvalues $\lambda_{\min}$ and $\lambda_{\max}$. The remaining positive constants $\underline{c}$ and $\overline{c}$ have no dependence on δ, h, and s.

For $\lambda_{\min}$, we utilize the *nonlocal characterization of Sobolev spaces* introduced in [10] and related results from [45]. This nonlocal characterization of Sobolev spaces has been used for solving variational problems arising in image diffusion applications; see [7] and the references therein. We obtain sharp quantification of parameters of $\lambda_{\min}$. In addition, we verify the sharpness of quantification of $\lambda_{\min}$ by exploiting the Toeplitz property of the stiffness matrix.

For $\lambda_{\max}$, we first use norm estimates. However, it turns out that the resulting quantifications are not sharp. The norm estimate technique is valid for any spatial dimension, but sharp quantification is lost because the inverse estimate obscures dependence on the parameters. To achieve sharpness, we take an "invasive" algebraic approach and work with matrix entries directly since the condition number is mostly an algebraic quantity. This matrix based analysis is relatively simple, yet powerful, and it seems to be a more holistic and effective approach in our case. We achieve sharp quantifications of $\lambda_{\max}$ through the use of the Gerschgorin circle theorem.

The rest of the article is structured as follows. In Section 2, we discuss a convenient scaling of the operator which prevents degeneracy of the nonlocal operator and provides its convergence to the local one. In Section 3, we present the sharp quantification of $\lambda_{\min}$ in (1.6) through the nonlocal characterization of Sobolev spaces. In Section 4, we use norm estimates to find a quantification of $\lambda_{\max}$. In Section 5, we utilize two popular discretizations: piecewise constant and linear finite elements. We carefully construct the stiffness matrix entries and establish its Toeplitz property. In Section 6, we achieve the sharpness of the quantification of all parameters of $\lambda_{\max}$ in (1.6) and provide the numerical verification of sharpness. The Toeplitz property opens another gateway to numerical linear algebra and in Section 7, we verify the sharpness of $\lambda_{\min}$ obtained in Section 3 algebraically and numerically. In Section 8, we visit the integrable kernel case and provide sharp quantification of $\lambda_{\min}$ and $\lambda_{\max}$ by recovering the missing h-quantification from the first author's earlier work [2, 3]. Finally, we conclude in Section 9.

2. Scaling of the operator and convergence to the local case. The general form of the operator $\mathcal{L}$ in (1.2) involves a scaling factor c_δ which is obtained from an energy estimate. To be precise, it is derived from a comparison of the deformation energy density in the PD framework to the energy in the classical linear elasticity, as pointed out in [24, 25, 55]. The energy estimate enforces the following:

$$\tau_\delta := c_\delta \int_{B_\delta(0)} \frac{1}{|x|^{d+2s}}|x|^2 dx < +\infty. \tag{2.1}$$

The condition (2.1) allows for a wide choice of c_δ. The choice of

$$c_\delta^{-1} := \frac{1}{\omega_d}\int_{B_\delta(0)} \frac{1}{|x|^{d+2s}}|x|^2 dx = \frac{\delta^{2-2s}}{2-2s} \tag{2.2}$$

as a scaling factor in (1.2) leads to a more specialized energy estimate than (2.1):

$$\tau_\delta = \omega_d, \tag{2.3}$$

where ω_d denotes the surface area of the unit sphere in $\mathbb{R}^d$. There are several justifications for the convenience of the choice in (2.2). Since PD is a nonlocal extension of classical solid mechanics, one expects the convergence of the nonlocal operator to the local one as $\delta \to 0$. Hence, as we will show next, this choice corresponds to the additional constraint that the nonlocal operator converges to the local operator when $\delta \to 0$. The exact choice in (2.2) immediately guarantees the positive definiteness (nondegeneracy) of $\mathcal{L}$ as $\delta \to 0$. Similar convergence arguments related to scaling have been discussed in the literature; see [35, Chap. 9], [49]. In 1D and for $u \in C^4(\overline{\overline{\Omega}})$, using a change of variable together with a simple perturbation expansion reveal the convergence to the local operator [1]:

$$\begin{aligned}\mathcal{L}u(x) &= -c_\delta \int_0^\delta \frac{u(x+e)-2u(x)+u(x-e)}{e^{1+2s}}de \\ &= -c_\delta\{\frac{\delta^{2-2s}}{2-2s}u''(x)+\mathcal{O}(\delta^{4-2s})\} = -u''(x)+\mathcal{O}(\delta^2).\end{aligned}$$

Furthermore, denoting the local bilinear form by

$$\ell(u(x),u(x)) = (u'(x),u'(x))$$

and by using integration by parts with a homogeneous Dirichlet boundary condition, the bilinear form converges to the local bilinear form as $\delta \to 0$:

$$\begin{aligned}a(u,u) = (\mathcal{L}u,u) &= c_\delta\{\frac{\delta^{2-2s}}{2-2s}\ell(u,u)+\mathcal{O}(\delta^{4-2s})\} \\ &= \ell(u,u)+\mathcal{O}(\delta^2).\end{aligned}$$

We can also observe the convergence of eigenvalues. Let us consider the eigenvalues of the local operator with $u(0) = u(\pi) = 0$ and the eigenvalues of the odd periodic nonlocal operator. The eigenpairs are $(k^2, \sin(kx))$ and

$$(c_\delta \int_{-\delta}^{\delta} \frac{1}{|y|^{1+2s}}(1-\cos(ky))dy, \sin(kx)), \tag{2.4}$$

respectively. Again, by devising a perturbation expansion for $\cos(ky)$ and rearranging the integral, we observe that nonlocal eigenvalues converge to the local ones:

$$c_\delta \int_{-\delta}^{\delta} \frac{(1-\cos(ky))}{|y|^{1+2s}}dy = c_\delta\{k^2\frac{\delta^{2-2s}}{2-2s}+\mathcal{O}(\delta^{4-2s})\} = k^2+\mathcal{O}(\delta^2).$$

In addition, (2.2) eliminates the δ and s dependence of $\lambda_{\min}$ and as shown in Lemma 3.4, $\lambda_{\min}$ depends only on h. Hence, the δ- and s-quantifications of the condition number reduce to that of $\lambda_{\max}$; see Section 3.

[1] Throughout the article, the "local problem" refers to the 1D Laplace problem with homogeneous boundary conditions.

3. Minimal eigenvalue and nonlocal characterization of Sobolev spaces. In order to reveal the δ-quantification of the minimal eigenvalue, we prove a nonlocal Poincaré's inequality. The main ingredient leading to the δ-quantification is a *nonlocal characterization of Sobolev spaces* introduced in [10, 45]. First we recall the standard local Poincaré's inequality:

$$\|u\|_{L^2(\Omega)} \leq c_{Pncr} \|\nabla u\|_{L^2(\Omega)} \tag{3.1}$$

holds true for all $u \in H^1(\Omega)$ satisfying either

$$\int_\Omega u \, dx = 0 \quad \text{or} \quad |\{x \in \Omega : u(x) = 0\}| = \mu > 0.$$

The constant c_{Pncr} depends only on d, μ and Ω and we assume that it is the smallest constant. The nonlocal Poincaré-type inequality obtained in [10, 45] utilizes the sequence of radial functions ρ_n satisfying the following conditions:

$$\rho_n \geq 0 \quad \text{a.e. in } \mathbb{R}^d \quad \text{(nonnegativity)}, \tag{3.2a}$$

$$\int_{\mathbb{R}^d} \rho_n(x)dx = 1, \quad \forall n \geq 1 \quad \text{(probability measure)}, \tag{3.2b}$$

$$\lim_{n\to\infty} \int_{|t|>r} \rho_n(t)dt = 0, \quad \forall r > 0 \quad \text{(decay)}. \tag{3.2c}$$

For a pure Neumann boundary condition setting, a nonlocal Poincaré-type inequality was proved in [45]. In [2], the first author generalized this result to cover spaces that come with mixed boundary condition:

$$V_M := \{v \in L^2(\overline{\overline{\Omega}}) : v = 0 \text{ on } \mathcal{B}\Omega_e\}.$$

The set $\mathcal{B}\Omega_e$ refers to the portion of the boundary where a Dirichlet boundary condition is imposed. We denote the complement $\mathcal{B}\Omega \setminus \mathcal{B}\Omega_e$ by $\mathcal{B}\Omega_n$. In particular, also in [2], we have given the nonlocal Poincaré-type inequality for V_D as below:

LEMMA 3.1. *For any $\eta > 0$, there exists n_0 such that*

$$\|u\|^2_{L^2(\overline{\overline{\Omega}})} \leq \left(\frac{c_{Pncr}}{k_d} + \eta\right) \int_{\overline{\overline{\Omega}}} \int_{\overline{\overline{\Omega}}} \frac{|u(x) - u(y)|^2}{|x-y|^2} \rho_n(|x-y|) \, dydx \tag{3.3}$$

for all $u \in V_D$ and $n \geq n_0$. Here k_d is a constant that depends only on d.

The proof of Lemma 3.1 relies on the following compactness result and follows from [2, Lemma 3.2] by replacing V_M by V_D:

LEMMA 3.2. *If $(u_n) \subset V_D$ is a bounded sequence in $L^2(\overline{\overline{\Omega}})$ such that*

$$\int_{\overline{\overline{\Omega}}} \int_{\overline{\overline{\Omega}}} \frac{|u_n(x) - u_n(y)|^2}{|x-y|^2} \rho_n(|x-y|) \, dydx \leq b_0 \quad \forall n \geq 1,$$

then the following statements hold:

(i) (u_n) is relatively compact in $L^2(\overline{\overline{\Omega}})$.

(ii) If $u \in L^2(\overline{\overline{\Omega}})$ and $u_{n_j} \to u$ in $L^2(\overline{\overline{\Omega}})$, then $u \in H^1(\overline{\overline{\Omega}}) \cap V_D$.

(iii) Moreover, the limit function u satisfies the following gradient estimate: $\int_{\overline{\overline{\Omega}}} |\nabla u|^2 \leq b_0/k_d$.

Proof. The results follow from [45, Thm 1.2] and the fact that V_D is a closed subspace of $L^2(\overline{\overline{\Omega}})$. ∎

We obtain both the coercivity of the bilinear form $a(\cdot,\cdot)$ and the δ-quantification of the minimal eigenvalue by utilizing a specialized choice of mollifiers as follows:

COROLLARY 3.3. *For $a(\cdot,\cdot)$ given in (1.4), there exist $\delta_0 = \delta_0(\overline{\overline{\Omega}}) > 0$ and $\underline{\lambda} = \underline{\lambda}(\overline{\overline{\Omega}}, \delta_0) > 0$ such that for all $0 < \delta < \delta_0$ and $u \in V_D$:*

$$\underline{\lambda} \, \|u\|^2_{L^2(\overline{\overline{\Omega}})} \leq a(u,u). \tag{3.4}$$

Proof. Choose the radial mollifiers satisfying the conditions (3.2) as follows:

$$\rho_\delta(t) = \frac{1}{\omega_d} \frac{2-2s}{\delta^{2-2s}} t^{-d+2(1-s)} \chi_\delta(t), \quad \text{with } \chi_\delta(t) := \begin{cases} 1, & t \in B_\delta(0) \\ 0, & \text{otherwise.} \end{cases} \tag{3.5}$$

Then, (3.3) yields:

$$\begin{aligned} \|u\|^2_{L^2(\overline{\overline{\Omega}})} &\leq (\frac{c_{Pncr}}{k_d} + \eta) \frac{2}{\omega_d} \left\{ \frac{1-s}{\delta^{2-2s}} \int_{\overline{\overline{\Omega}}} \int_{\overline{\overline{\Omega}} \cap |x-y| \leq \delta} \frac{|u(x)-u(y)|^2}{|x-y|^{d+2s}} dy dx \right\} \\ &= \underline{\lambda}^{-1} a(u,u). \end{aligned} \tag{3.6}$$

∎

We are in a position to establish the sharpness up to a constant of the quantification given in (1.6) in 1D:

$$\lambda_{\min} = \underline{c} h. \tag{3.7}$$

LEMMA 3.4. *There exist positive constants c_* and c^* independent of δ, h, and s such that*

$$c_* h \leq \lambda_{\min} \leq c^* h.$$

Proof. Equation (3.6) implies that $\lambda_{\min}$ is bounded from below by a constant c_* independent of all three parameters:

$$c_* h \leq \lambda_{\min}.$$

For the upper bound, let $\Omega = (0,1)$ and choose

$$u(x) = \begin{cases} x, & x \in \Omega \\ 0, & x \in \mathcal{B}\Omega. \end{cases}$$

Clearly, $u \in V_D(\overline{\overline{\Omega}})$. We utilize linear finite element discretization of u with the following basis functions:

$$\phi_i(x) = \begin{cases} \frac{1}{h}(x - x_{i-1}), & x \in [x_{i-1}, x_i], \\ \frac{1}{h}(x_{i+1} - x), & x \in [x_i, x_{i+1}], \\ 0, & \text{otherwise,} \end{cases} \tag{3.8}$$

on a uniform mesh with mesh size h, i.e., with $x_i = ih, \quad i = 1, \dots, N$ and $h = 1/N$; also see the mesh depicted in Figure 5.1. The discretization of u yields:

$$u_h(x) = \sum_{i=1}^{N} ih\phi_i(x).$$

Hence, the coordinates of u_h satisfy $\left(\underline{u_h}\right)_i = ih$. Then, we obtain:

$$\lambda_{\min} \leq \frac{a(u_h, u_h)}{\underline{u_h}^t \underline{u_h}} = \frac{1}{h^2 \sum_{i=1}^{N} i^2} = \frac{1}{h^2 \frac{N(N+1)(2N+1)}{6}} \leq 3h.$$

□

In fact, by using Toeplitz matrix tools, it can be shown that the above constant $\underline{c}$ approaches π^2 as $N \to \infty$; see (7.7).

REMARK 3.5. *One can generalize the minimal eigenvalue estimate to a more general kernel family such as* $\frac{C(|x-y|)}{|x-y|^{d+2s}}$ *where* $C(|x-y|)$ *is a nonnegative, locally integrable function. Kernels similar to this family have also been studied; see [14, Eqn. (4.10)].*

The following choice of mollifiers allows such a generalization:

$$\rho_\delta(t) = \frac{1}{\omega_d} \frac{2(1-s)}{\delta^{2-2s}} t^{-d+2(1-s)} \gamma(t/\delta),$$

where $\gamma(|x-y|)$ *is nonnegative, locally integrable, and compactly supported.*

When enforcing the probability measure condition for ρ_δ *in (3.2), the scaling by* $1/\delta$ *in the argument of* γ*, i.e.,* t/δ*, eliminates* δ^{2-2s}*. This yields the following (moment) condition which is independent of* δ *and allows the condition to hold for all* $\delta > 0$*, in particular for* $\delta \to 0$*.*

$$2(1-s) \int_0^\infty \gamma(t) t^{1-2s} dt = 1.$$

Then, the lower bound of the minimal eigenvalue similar to (3.6) follows immediately by letting $C(|x-y|) := \gamma(|x-y|/\delta)$*. This argument has also been used by the first author to generalize minimal eigenvalue estimates for integrable kernel cases [2, Eqn. (3.4)].*

4. Maximal eigenvalue bounds using norm estimates. Our main goal is to obtain δ-, h-, and s-quantifications of the maximal eigenvalue. In this pursuit, we exploit two norm estimates: $a(u,u) \leq c\|u\|^2_{H^1}$ and $a(u,u) \leq c\|u\|^2_{H^s}$. The constants in those norm estimates will serve as quantification constants. For $a(u,u) \leq c\|u\|^2_{H^1}$, we start the construction with the same regularity assumption of the local case, i.e., $u \in H^1(\overline{\overline{\Omega}})$. This is a more restrictive regularity assumption than what we have utilized so far.

PROPOSITION 4.1. *Let* $\Omega \subset \mathbb{R}^d$ *be of class* $C^{0,1}$ *Lipschitz continuous,* $u \in H^1(\overline{\overline{\Omega}})$*, and* $a(\cdot,\cdot)$ *be given as in (1.4). Then,*

$$a(u,u) \leq c\|u\|^2_{H^1(\overline{\overline{\Omega}})}. \tag{4.1}$$

Proof. The proof is valid for general dimension d. For simplicity, we omit the factors (2.2) and $\frac{1}{2}$ in front of the bilinear form (1.4). Utilizing the regularity assumption on Ω, one can extend u to a function $\tilde{u} : \mathbb{R}^d \to \mathbb{R}$ such that $u \in H^1(\mathbb{R}^d)$ and $\|\tilde{u}\|_{H^1(\mathbb{R}^d)} \leq c\|u\|_{H^1(\overline{\overline{\Omega}})}$.

$$
\begin{aligned}
&\int_{\overline{\overline{\Omega}}} \int_{\overline{\overline{\Omega}} \cap |x-y| \leq \delta} \frac{(u(y)-u(x))^2}{|y-x|^{d+2s}} dydx \\
&\leq \int_{\overline{\overline{\Omega}}} \int_{|x-y| \leq \delta} \frac{(\tilde{u}(y)-\tilde{u}(x))^2}{|y-x|^{d+2s}} dydx \\
&= \int_{\overline{\overline{\Omega}}} \int_{|e| \leq \delta} \frac{1}{|e|^{d+2(s-1)}} \left(\frac{\tilde{u}(x+e)-\tilde{u}(x)}{|e|} \right)^2 dedx \\
&\leq \int_{\overline{\overline{\Omega}}} \int_{|e| \leq \delta} \frac{1}{|e|^{d+2(s-1)}} \left(\int_0^1 |\nabla \tilde{u}(x+te)| dt \right)^2 dedx \\
&\leq \int_0^1 \int_{|e| \leq \delta} \frac{1}{|e|^{d+2(s-1)}} \left(\int_{\mathbb{R}^d} |\nabla \tilde{u}(x+te)|^2 dx \right) dedt \\
&= ||\nabla \tilde{u}||^2_{L^2(\mathbb{R}^d)} \int_{|e| \leq \delta} \frac{1}{|e|^{d+2(s-1)}} de \\
&= ||\nabla \tilde{u}||^2_{L^2(\mathbb{R}^d)} \omega_d \frac{\delta^{2-2s}}{2-2s} \\
&\leq c\delta^{2-2s} ||u||^2_{H^1(\overline{\overline{\Omega}})}.
\end{aligned}
$$

The result follows after incorporating the scaling in (2.2).
□

Let $\lesssim$ denote the following relation: $P \lesssim Q$ if and only if there exists a positive constant c such that $P \leq c\,Q$. Let $\underline{u}$ denote the l^2-coordinates of u with respect to the linear finite element discretization. Then the well-conditioning property of the mass matrix leads to the following well-known norm equivalence:

$$
h^d \|\underline{u}\|^2_{l^2} \lesssim \|u\|^2_{L^2} \lesssim h^d \|\underline{u}\|^2_{l^2}. \tag{4.2}
$$

By the help of $\lesssim$ notation, we can also suppress the involved constants in the inverse inequality:

$$
\|u\|^2_{H^s(\overline{\overline{\Omega}})} \lesssim h^{-2s} \|u\|^2_{L^2(\overline{\overline{\Omega}})}, \quad s \in [0,1].
$$

Remark 4.2. *Let $V_D^h(\overline{\overline{\Omega}})$ be the finite element space corresponding to $V_D(\overline{\overline{\Omega}})$. After using the inverse inequality, (4.1) implies that*

$$
a(u,u) \lesssim h^{-2} \|u\|^2_{L^2(\overline{\overline{\Omega}})}, \quad u \in V_D^h(\overline{\overline{\Omega}}). \tag{4.3}
$$

Combining (3.6) with (4.3), we arrive at the nonlocal spectral equivalence:

$$
1 \lesssim \frac{a(u,u)}{\|u\|^2_{L^2(\overline{\overline{\Omega}})}} \lesssim h^{-2}. \tag{4.4}
$$

It is interesting to note that (4.4) is similar to the spectral equivalence in the local case:

$$
1 \lesssim \frac{\ell(u,u)}{\|u\|^2_{L^2(\Omega)}} \lesssim h^{-2}.
$$

In Proposition 4.1, enforcing the same regularity assumption of the local case, i.e., $u \in H^1(\overline{\overline{\Omega}})$, creates a resemblance to the local case totally obscuring *δ-quantification. (4.3) is undesirable, but serves as a "default" upper bound.*

By simply relaxing the restriction $\overline{\overline{\Omega}} \cap |x-y| \leq \delta$ in the inner integral of (1.4), we can obtain an improved upper bound:

$$a(u,u) \leq \frac{1-s}{\delta^{2-2s}} |u|^2_{H^s(\overline{\overline{\Omega}})}. \tag{4.5}$$

We can use the inverse inequality after restricting u to $V_D^h(\overline{\overline{\Omega}})$. Then in 1D, (4.5) and (4.2) with $d=1$ yield:

$$\begin{aligned} a(u,u) &\leq \frac{1-s}{\delta^{2-2s}} \|u\|^2_{H^s(\overline{\overline{\Omega}})} \\ &\lesssim h^{-2s}\delta^{-(2-2s)} \|u\|^2_{L^2(\overline{\overline{\Omega}})} \\ &\lesssim h^{1-2s}\delta^{-(2-2s)} \|\underline{u}\|^2_{l^2}. \end{aligned} \tag{4.6}$$

The ratio of the horizon and the mesh size plays a crucial role in our analysis. Hence, we define:

$$R = \frac{\delta}{h}. \tag{4.7}$$

Then, (4.6) yields:

$$\lambda_{\max} \lesssim h^{1-2s}\delta^{-(2-2s)} = \frac{1}{R^{2-2s}} h^{-1}. \tag{4.8}$$

On the other hand, (4.1) yields:

$$\lambda_{\max} \lesssim h^{-1} \tag{4.9}$$

Suppressing the dependencies in the involved constants, (4.8) becomes a better bound than (4.9). Furthermore, note that (4.9) can be obtained from (4.8) by assuming $u \in H^1(\overline{\overline{\Omega}})$ and taking the limit of (4.8) as $s \to 1$. But, neither (4.8) nor (4.9) is sharp; see the discussion at the end of Section 6.

5. Discretization and stiffness matrix entries. The weak form is obtained in the usual way; by testing the strong form of the operator (1.2). More precisely,

$$a(u,v) = (\mathcal{L}u, v) = -\frac{2-2s}{\delta^{2-2s}} \int_{\overline{\overline{\Omega}}} \int_{\overline{\overline{\Omega}} \cap |x-y| \leq \delta} \frac{u(y)-u(x)}{|x-y|^{d+2s}} v(x) dy dx. \tag{5.1}$$

The two bilinear forms (1.4) and (5.1) are equivalent; see [3, Eqn. (3.4)]. However, we use (5.1) in the stiffness matrix construction because it offers the following convenient property. When $u \in V_D(\overline{\overline{\Omega}})$, the outer integration limit reduces from $\overline{\overline{\Omega}}$ to Ω. Furthermore, the inner integration limit $\{y : \overline{\overline{\Omega}} \cap |x-y| \leq \delta\}$ simply becomes $\{y : |x-y| \leq \delta\}$.

We present the stiffness matrix construction based on linear finite element discretization for the domain $\Omega = (0,1)$. The corresponding nonlocal closure of Ω becomes $\overline{\overline{\Omega}} = [-\delta, 1+\delta]$. Define the interval of influence of a node x_i as

$$I_{x_i} := [x_{i-1} - \delta, x_{i+1} + \delta] \cap \overline{\overline{\Omega}}. \tag{5.2}$$

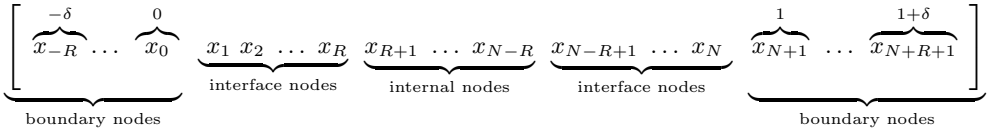

FIG. 5.1. *The nonlocal finite element mesh where the node locations are denoted by* x_i, $i = -R, \ldots, N+R+1$, *where* $\overline{\overline{\Omega}} = [-\delta, 1+\delta]$.

Due to radial property, hence, translation invariance, of the kernel function in (1.2), we establish the following important property of the stiffness matrix.

LEMMA 5.1. *The stiffness matrix is a Toeplitz matrix. Namely,* $A_{i,j} = A_{i+1,j+1}$.

Proof. We use the equivalent bilinear form given in (5.1). We assume a uniform mesh with mesh size h. Then, substituting $\bar{x} = x + h, \bar{y} = y + h$ and denoting the support of $\phi_i(x)$ by $[x_{i-1}, x_{i+1}]$, we get:

$$
\begin{aligned}
A_{i,j} = a(\phi_i, \phi_j) &= -\frac{2-2s}{\delta^{2-2s}} \int_{x_{i-1}}^{x_{i+1}} \int_{x-\delta}^{x+\delta} \frac{[\phi_j(y) - \phi_j(x)]\phi_i(x)}{|x-y|^{1+2s}} dy dx \qquad (5.3)\\
&= -\frac{2-2s}{\delta^{2-2s}} \int_{x_{i-1}+h}^{x_{i+1}+h} \int_{\bar{x}-\delta}^{\bar{x}+\delta} \frac{[\phi_j(\bar{y}-h) - \phi_j(\bar{x}-h)]\phi_i(\bar{x}-h)}{|\bar{x}-h-(\bar{y}-h)|^{1+2s}} d\bar{y} d\bar{x}\\
&= -\frac{2-2s}{\delta^{2-2s}} \int_{x_i}^{x_{i+2}} \int_{\bar{x}-\delta}^{\bar{x}+\delta} \frac{[\phi_{j+1}(\bar{y}) - \phi_{j+1}(\bar{x})]\phi_{i+1}(\bar{x})}{|\bar{x}-\bar{y}|^{1+2s}} d\bar{y} d\bar{x}\\
&= A_{i+1,j+1}.
\end{aligned}
$$

□

We study the nonzero structure of the stiffness matrix. Due to the symmetry of the bilinear form and the Toeplitz property of the stiffness matrix, we concentrate only on the first row.

LEMMA 5.2. *Let* R *be the ratio in* (4.7). *The number of nonzero entries in the first row of the stiffness matrix is* $R+2$.

Proof. The nonzero entries arise due to the interaction of basis functions. For this reason, we concentrate on the numerator of the integrand in (5.3). Since we compute the first row, i.e., $i = 1$, the two terms we concentrate are $\phi_j(x)\phi_1(x)$ and $\phi_j(y)\phi_1(x)$. The first term $\phi_1(x)\phi_j(x) \neq 0$ for $j = 1, 2$. The other term $\phi_1(x)\phi_j(y)$ has a 2D support. Namely, $\phi_1(x)\phi_j(y) \neq 0$ on $(x, y) \in [x_0, x_2] \times [x_{j-1}, x_{j+1}]$. The inner integration limit $y \in [x-\delta, x+\delta]$ enforces an additional constraint. Furthermore, basis functions $\phi_j(y), j = 1, \ldots, N$ have support $y \in [0, 1]$ for $\Omega = (0, 1)$; see Figure 5.1. So, the limits of integration for y becomes $[0, x+\delta]$. Hence, the support $\phi_1(x)\phi_j(y)$ reduces to the following:

$$
(x, y) \in [x_0, x_2] \times [x_{j-1}, x_{j+1}] \cap [x_0, x_2] \times \{y : 0 \leq y \leq x + \delta\}. \qquad (5.4)
$$

The indices satisfying (5.4) are exactly $j = 1, \ldots, R, R+1, R+2$. The union of the indices obtained from the first term, i.e., $j = 1, 2$ and that second term leads to $j = 1, \ldots, R, R+1, R+2$. Consequently, we end up with $R+2$ nonzero entries in the first row. □

The construction of the stiffness matrix is based on the types of nodes. The nodes are classified into three groups: boundary, interface, and internal; see Figure 5.1:

$$\begin{aligned} \text{internal:} \quad & \{x_i \in \Omega : I_{x_i} \subset \Omega\}, \\ \text{interface:} \quad & \{x_i \in \Omega : I_{x_i} \subset \overline{\overline{\Omega}} \text{ and } I_{x_i} \not\subset \Omega\}, \\ \text{boundary:} \quad & \{x_i \in \overline{\overline{\Omega}} \setminus \Omega\}. \end{aligned}$$

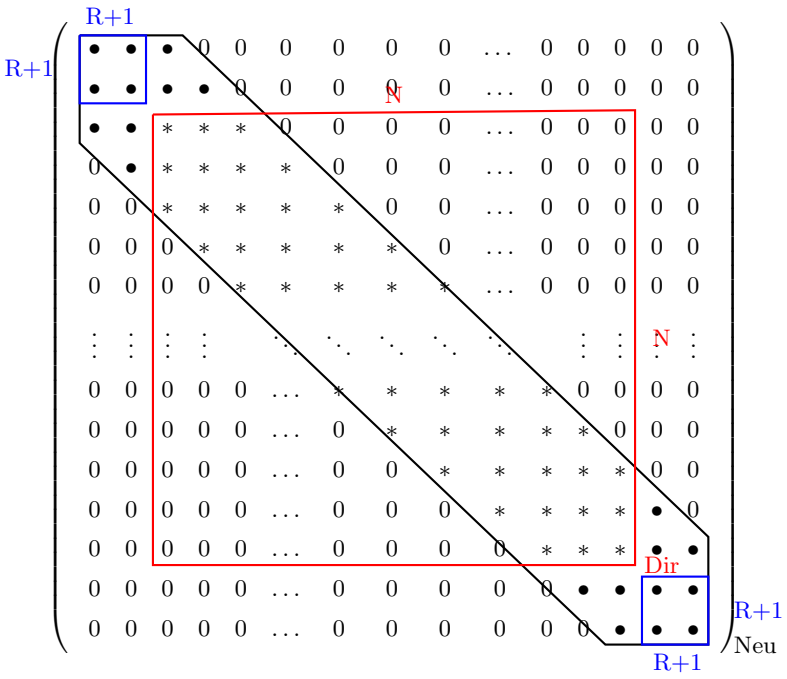

FIG. 5.2. *The sparsity structure of the Dirichlet and Neumann stiffness matrices. The rows and columns in the blue boxes (i.e., boundary nodes) of the Neumann matrix are deleted to obtain the Dirichlet matrix enclosed by the red box.*

We explain the construction of the (Dirichlet) stiffness matrix. The sparsity structure of the Neumann matrix and the corresponding Dirichlet matrix is given below. The Neumann matrix includes all three types of nodes, whereas the Dirichlet matrix is extracted from the Neumann one by deleting the boundary nodes as in the local case. Due to the nonlocal boundary condition, the Neumann matrix of size $N + 2R + 2$ shrinks to Dirichlet matrix of size N after deletion; see Figure 5.2.

Observe that the interval of influence of the boundary nodes is nested. Namely, $I_{x_{k-1}} \subset I_{x_k}$, $k = -R+1, \ldots, 0$. As a result, the diagonal entry values of each row increase, i.e., $A_{k-1,k-1} < A_{k,k}$, $k = -R+1, \ldots, 0$. This causes the Neumann matrix to lose the Toeplitz property in the rows corresponding to boundary nodes.

We now explain how the entries can be calculated by utilizing the following splitting for the interior nodes, the others easily follow. For simplicity, we omit the factors (2.2) in front of the bilinear form (5.1):

(a) piecewise linear for $s \in (0,1)$

$A_{1,1}$	$\delta^{-1}\left(\frac{4(2^{1-2s}-1)}{s(1-2s)(3-2s)R^{1-2s}} - \frac{4(1-s)}{3sR}\right)$	≥ 0
$A_{1,2}$	$\delta^{-1}\left(\frac{(7-4\times 2^{3-2s}+3^{3-2s})}{2s(1-2s)(3-2s)R^{1-2s}} - \frac{1-s}{3sR}\right)$	≤ 0
$A_{1,j+1}$	$\delta^{-1}\frac{(j-2)^{3-2s}-4(j-1)^{3-2s}+6j^{3-2s}-4(j+1)^{3-2s}+(j+2)^{3-2s}}{2s(1-2s)(3-2s)R^{1-2s}}, \quad 2 \leq j \leq R-2$	≤ 0
$A_{1,R}$	$\delta^{-1}\left(\frac{(R-3)^{3-2s}-4(R-2)^{3-2s}+6(R-1)^{3-2s}-\frac{3(R-1)}{R}R^{3-2s}-2sR^{2-2s}}{2s(1-2s)(3-2s)R^{1-2s}} + \frac{(3R+1)(1-s)}{6sR} + \frac{1-s}{1-2s}\right)$	≤ 0
$A_{1,R+1}$	$\delta^{-1}\left(\frac{\left((R-2)^{3-2s}-4(R-1)^{3-2s}+\frac{3(R-2)}{R}R^{3-2s}+4sR^{2-2s}\right)}{2s(1-2s)(3-2s)R^{1-2s}} + \frac{1-s}{3sR}\right)$	≤ 0
$A_{1,R+2}$	$\delta^{-1}\left(\frac{(R-1)^{3-2s}-\frac{(R-3)}{R}R^{3-2s}-2sR^{2-2s}}{2s(1-2s)(3-2s)R^{1-2s}} - \frac{(3R-1)(1-s)}{6sR} - \frac{1-s}{1-2s}\right)$	≤ 0

(b) piecewise constant for $s \in (0, \frac{1}{2})$

$A_{1,1}$	$\delta^{-1}\left(\frac{2(1-s)}{s(1-2s)R^{1-2s}} - \frac{2(1-s)}{sR}\right)$	≥ 0
$A_{1,j+1}$	$\delta^{-1}\frac{\left((j-1)^{1-2s}-2j^{1-2s}+(j+1)^{1-2s}\right)(1-s)}{s(1-2s)R^{1-2s}}, \quad 1 \leq j \leq R-1$	≤ 0
$A_{1,R+1}$	$\delta^{-1}\left(\frac{\left((R-1)^{1-2s}-R^{1-2s}\right)(1-s)}{s(1-2s)R^{1-2s}} + \frac{1-s}{sR}\right)$	≤ 0

TABLE 5.1

Stiffness matrix entries constructed by the corresponding finite element discretization for the singular kernel. Diagonal entries are positive and off-diagonal ones are negative.

$$
\begin{aligned}
&-\int_{x_{i-1}}^{x_{i+1}}\int_{x-\delta}^{x+\delta}\frac{[\phi_j(y)-\phi_j(x)]\phi_i(x)}{|x-y|^{1+2s}}dydx = \\
&-\int_{x_{i-1}}^{x_i}\int_{x-\delta}^{x_{j-1}}\frac{[-\phi_j(x)]\phi_i(x)}{|x-y|^{1+2s}}dydx - \int_{x_i}^{x_{i+1}}\int_{x-\delta}^{x_{j-1}}\frac{[-\phi_j(x)]\phi_i(x)}{|x-y|^{1+2s}}dydx \\
&-\int_{x_{i-1}}^{x_i}\int_{x_{j-1}}^{x_j}\frac{[\phi_j(y)-\phi_j(x)]\phi_i(x)}{|x-y|^{1+2s}}dydx - \int_{x_i}^{x_{i+1}}\int_{x_{j-1}}^{x_j}\frac{[\phi_j(y)-\phi_j(x)]\phi_i(x)}{|x-y|^{1+2s}}dydx \\
&-\int_{x_{i-1}}^{x_i}\int_{x_j}^{x_{j+1}}\frac{[\phi_j(y)-\phi_j(x)]\phi_i(x)}{|x-y|^{1+2s}}dydx - \int_{x_i}^{x_{i+1}}\int_{x_j}^{x_{j+1}}\frac{[\phi_j(y)-\phi_j(x)]\phi_i(x)}{|x-y|^{1+2s}}dydx \\
&-\int_{x_{i-1}}^{x_i}\int_{x_{j+1}}^{x+\delta}\frac{[-\phi_j(x)]\phi_i(x)}{|x-y|^{1+2s}}dydx - \int_{x_i}^{x_{i+1}}\int_{x_{j+1}}^{x+\delta}\frac{[-\phi_j(x)]\phi_i(x)}{|x-y|^{1+2s}}dydx, \quad j=i+2,\ldots,i+R-2.
\end{aligned}
\tag{5.5}
$$

We utilize two types of discretizations: linear and constant finite elements. The linear finite element basis functions are given in (3.8). The constant finite element

ones with a uniform mesh size h are as follows:

$$\phi_i(x) = \begin{cases} 1, & x \in [x_i - h/2, x_i + h/2], \\ 0, & \text{otherwise}, \end{cases}$$

The value of the stiffness matrix entries obtained are listed in Table 5.1.

REMARK 5.3. *Symbolic computation in Mathematica was used to obtain the matrix entries. There are eight integrals involved in the computation; see (5.5). Hence, coming up with a manageable formula for each entry is a nontrivial task. The introduction of R has significantly reduced the complexity of the algebra in Table 5.1.*

The matrix entry formulas in Tables 5.1 are valid for $s \in (0, 1/2) \cup (1/2, 1)$. The entries for the value of $s = 1/2$ are given by the limit.

5.1. Zero row sum property. The zero row sum property is an implication of the Neumann boundary condition as in the local case. The fact that

$$a(c, c) = 0, \tag{5.6}$$

for any nonzero constant function c in $\overline{\overline{\Omega}}$ is an analog of

$$\ell(c, c) = 0,$$

where, this time, the nonzero constant function c has domain $\overline{\Omega}$.

We immediately see that all rows of the Neumann matrix have zero sum due to property (5.6). This zero row sum property carries over to the rows of the Dirichlet matrix corresponding only to the internal nodes. The Dirichlet matrix is obtained by deleting the rows and columns corresponding to boundary nodes; see Figure 5.2. Since these nodes couple only with interface nodes, this deletion spoils the zero row sum property only for the rows corresponding to interface nodes, thereby, leaving the rows corresponding to the internal nodes unchanged.

5.2. Off-diagonal entries are negative. Establishing negativeness of the off-diagonal entries is involved and requires some algebra. We provide a relatively easy to follow case and prove the negativeness of $A_{1,j+1}$ where

$$A_{1,j+1} = \delta^{-1} \frac{(j-2)^{3-2s} - 4(j-1)^{3-2s} + 6j^{3-2s} - 4(j+1)^{3-2s} + (j+2)^{3-2s}}{2s(1-2s)(3-2s)R^{1-2s}}.$$

First, we decompose $A_{1,j+1}$: $A_{1,j+1} = p(s)h(j)$ where $p(s) := \frac{\delta^{-1}}{2s(1-2s)(3-2s)R^{1-2s}}$ and $h(j)$ is a composition of three functions in the following way: $f(x) := x^{3-2s}$, $g(x) := f(x-1) - 2f(x) + f(x+1)$, $h(x) := g(x-1) - 2g(x) + g(x+1)$ with $2 \le x \le R-2$.

We have to consider $s \in (0, 1/2)$ and $s \in (1/2, 1)$ separately.

- $s \in (0, 1/2)$: Since $p(s) \ge 0$, it remains to show that $h(x) < 0$.
  Note that $f(x) = x^{3-2s} > 0$, $f'(x) > 0$, $f''(x) > 0$, i.e., concave up and increasing. Then, $g(x) := \{f(x-1) - f(x)\} - \{f(x) - f(x+1)\} > 0$. Using the exact expression of $g(x)$, we arrive at the following:

  $$g'(x) = (3-2s)[\{(x-1)^{2-2s} - x^{2-2s}\} - \{x^{2-2s} - (x+1)^{2-2s}\}] > 0,$$
  $$g''(x) = (3-2s)(2-2s)[\{(x-1)^{1-2s} - x^{1-2s}\} - \{x^{1-2s} - (x+1)^{1-2s}\}] < 0.$$

  Hence, $g(x)$ is concave down and increasing, which results in $h(x) := \{g(x-1) - g(x)\} - \{g(x) - g(x+1)\} < 0$.

- $s \in (1/2, 1)$: Since $p(s) < 0$, it remains to show that $h(x) > 0$. In this case, $f(x) > 0$ is concave up and increasing, whereas $g(x) > 0$ is concave up and decreasing. Thus, the result follows.

The rest of the off-diagonal entries can be proved to be negative by using similar algebraic techniques.

REMARK 5.4. *The coercivity of the bilinear form implies that the eigenvalues of A are positive. This property with the negativity of the off-diagonal entries implies that A is an M-matrix.*

5.3. Piecewise constant discretization. Sobolev embedding theorems [13] indicate that jump discontinuities belong to fractional Sobolev spaces $H^s(\overline{\overline{\Omega}})$ with $s \in [0, 1/2]$ in 1D. Hence, we study the piecewise constant finite element discretization as it naturally falls into the same fractional Sobolev space due to its inherent jump discontinuity. This discretization is relatively simple, but it captures the same δ-, h-, and s-quantifications of $\lambda_{\max}$ as the piecewise linear case; see $A_{1,1}$ entry in Table 5.1. Furthermore, it preserves the M-matrix property.

6. The comparison of the Gerschgorin bound and its sharpness. Denote the index for interior nodes by i_*. We have established that the rows corresponding to interior nodes have zero sum. Using this fact and the negativity of off-diagonal entries, we arrive at the following:

$$\begin{aligned} A_{i_*,i_*} &= -\sum_{j \neq i_*} A_{i_*,j} \\ &= \sum_{j \neq i_*} |A_{i_*,j}|. \end{aligned} \tag{6.1}$$

Observe that the set of nonzeros corresponding to an interior row is a superset corresponding to that of interface nodes. In fact, the interior rows contain the largest number of nonzeros. Hence,

$$\sum_{j \neq i} |A_{i,j}| \leq \sum_{j \neq i_*} |A_{i_*,j}| \tag{6.2}$$

The Gerschgorin circle theorem indicates the following:

$$|\lambda - A_{i,i}| \leq \sum_{j \neq i} |A_{i,j}|,$$

where λ is an eigenvalue of A. Then, using (6.2), $A_{i_*,i_*} = A_{i,i}$, and (6.1), we get:

$$\begin{aligned} |\lambda| &\leq A_{i,i} + \sum_{j \neq i} |A_{i,j}| \\ &\leq A_{i_*,i_*} + \sum_{j \neq i_*} |A_{i_*,j}| = 2A_{i,i}. \end{aligned} \tag{6.3}$$

Consequently, we have obtained an upper bound for the maximal eigenvalue.

REMARK 6.1. *In the local case, the off-diagonal entries are similarly negative. By the same argument above, the maximal eigenvalue can be bounded by twice the diagonal entry:*

$$\lambda_{\max}^{local} \leq c2h^{-1}.$$

The inverse inequality which is known to be sharp gives exactly the same h-quantification for the upper bound of the maximal eigenvalue. We will prove that the same Gerschgorin idea applied to the nonlocal case gives sharp δ-, h-, and s-quantifications of the maximal eigenvalue.

In the rest of the article, we will refer the Gerschgorin bound as G-bound. Note that dropping the negative term, the G-bound recovers (4.8):

$$\begin{aligned}\lambda_{\max} &\leq 2\delta^{-1}\left(\frac{4(2^{1-2s}-1)}{s(1-2s)(3-2s)R^{1-2s}} - \frac{4(1-s)}{3sR}\right) \\ &\leq \frac{c^+(s)}{R^{2-2s}}h^{-1}.\end{aligned} \tag{6.4}$$

Mainly, we aim to obtain δ- and h- quantification of the maximal eigenvalue. It is natural to obtain such quantification up to a constant. Since (4.8) lacks the negative term $-\frac{4(1-s)}{3sR}$, the G-bound is tighter. Next, we prove that it is sharp up to a constant which does not depend on s.

LEMMA 6.2.

$$A_{1,1} \leq \lambda_{\max} \leq 2A_{1,1} \tag{6.5}$$

Proof. The Gerschgorin circle theorem implies that (see (6.3))

$$\lambda_{\max} \leq 2A_{1,1}.$$

On the other hand, choose u to be the basis function corresponding to the first node x_1. Namely, $\underline{u} = e_1$ where e_1 is the first standard basis vector of dimension $N \times 1$:

$$\begin{aligned}A_{1,1} &= \frac{\underline{u}^t A \underline{u}}{\underline{u}^t \underline{u}} \\ &\leq \lambda_{\max}.\end{aligned}$$

□

REMARK 6.3. *The constant in the G-bound of $\lambda_{\max}$ can be improved by paying attention to the $\cos(kt)$ terms in (7.2) [29]:*

$$A_{1,1} + 2\sum_{j=2}^{R+2} |A_{1,j}| \cos\frac{\pi}{\lfloor \frac{N-1}{j-1} \rfloor + 2} \leq 2A_{1,1} = \ G\text{-bound}.$$

However, it would be quite cumbersome to extract a natural δ-, h-, and s-quantification of $\lambda_{\max}$ like the one G-bound provides when both off-diagonal terms and $\cos(kt)$ are involved. Due to this reason, we do not further pursue this estimate.

Combining (3.7) with (4.9) and (4.8), we obtain the following condition number bounds, respectively.

$$\kappa(A) \leq ch^{-2}, \tag{6.6}$$

$$\kappa(A) \leq ch^{-2s}\delta^{-(2-2s)}. \tag{6.7}$$

Using 1D Fourier analysis and directly using the eigenvalues of the nonlocal operator given in (2.4), a similar condition number bound capturing the cases above was first reported in [55, p. 1772] (also see [14, Eqn. (6.4)]):

$$\kappa(A) \leq c\min\{h^{-2s}\delta^{-(2-2s)}, h^{-2}\}. \tag{6.8}$$

Note that we obtain the estimates (6.6) and (6.7) from a different approach that allows generality in the sense that they are valid for d-dimensions.

The ability to increase mesh resolution freely is a desirable simulation property. Hence, the following setting is an important nonlocal regime:

$$h \ll \delta < 1. \tag{6.9}$$

When (6.9) holds, (6.8) defaults to (6.7). However, using (3.7) and (6.4), the condition number bound for 1D we obtained by the Gerschgorin estimate is sharp:

$$\kappa(A) \leq c^{+}(s)\, h^{-2s} \delta^{-(2-2s)} - c^{-}(s)\, \delta^{-2}, \tag{6.10}$$

where $c^{+}(s) := c\frac{8(2^{1-2s}-1)}{s(1-2s)(3-2s)}$ and $c^{-}(s) := c\frac{8(1-s)}{3s}$.

REMARK 6.4. *Note that* (6.10) *enjoys a superior feature which allows analysis of the behaviour of the bound with respect to the regularity parameter s. On the other hand, it would be difficult to reveal the s-quantification in the estimates* (6.6) *and* (6.7) *as they both depend on the inverse inequality.*

We also support the sharpness of the G-bound with numerical data; see Figure 6.1. $\lambda_{\max}$ (and $\lambda_{\min}$) values are computed in Matlab throughout the paper.

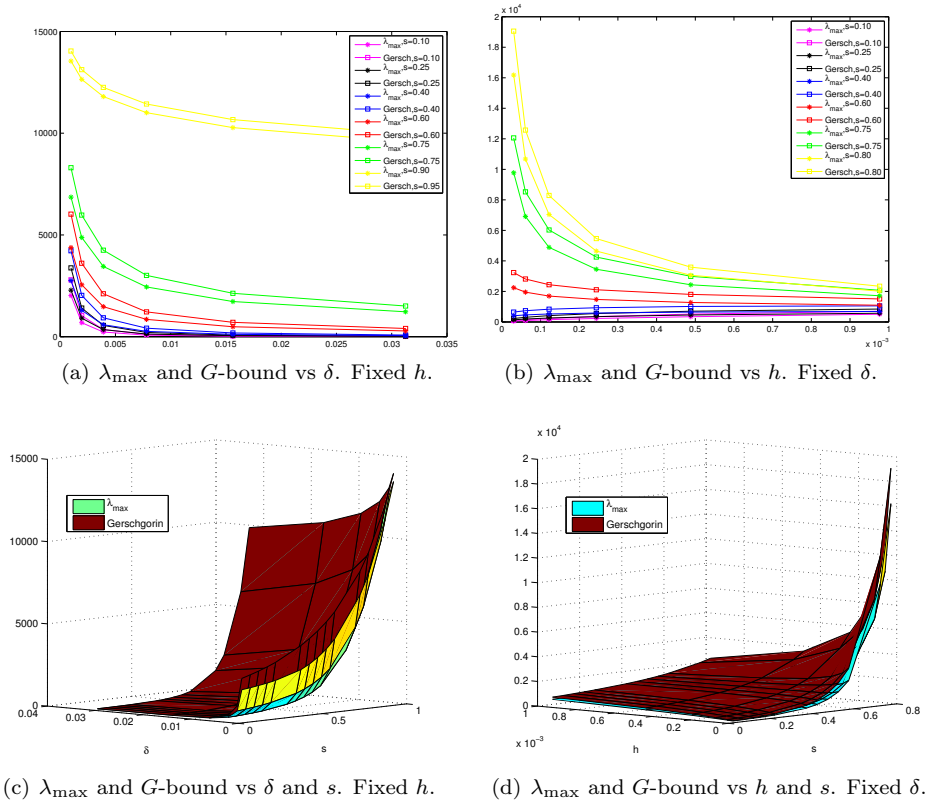

(a) $\lambda_{\max}$ and G-bound vs δ. Fixed h.

(b) $\lambda_{\max}$ and G-bound vs h. Fixed δ.

(c) $\lambda_{\max}$ and G-bound vs δ and s. Fixed h.

(d) $\lambda_{\max}$ and G-bound vs h and s. Fixed δ.

FIG. 6.1. *Comparison of $\lambda_{\max}$ and G-bound. Apparently G-bound is sharp up to a constant independent of s. $h = 1/2^{12}$ and $\delta = 1/2^{8}$ are the fixed values.*

7. An algebraic approach to the estimation of the minimal eigenvalue. In Lemma 5.2, we established that the stiffness matrix A is a banded Toeplitz matrix with full bandwidth $2R+3$. Here, we study the extremal eigenvalues of A in the context of banded Toeplitz matrices. See the excellent book on banded Toeplitz matrices [8]. A Toeplitz matrix of order N is associated with its symbol $b(t)$ (also called as the generating Laurent polynomial). $A = T_N(b)$ is constructed by its symbol:

$$b(t) = \sum_{k=-(R+1)}^{R+1} A_k t^k,$$

where t is on the unit circle and the polynomial coefficients are obtained by a Fourier transform as follows:

$$A_k = \frac{1}{2\pi}\int_{-\pi}^{\pi} b(e^{it})e^{-ikt}dt.$$

The coefficients determine the matrix entries in the following way:

$$A_{i,j} := A_{j-i}, \quad i,j = 1,\ldots,N.$$

Due to the bandedness of A, we have $A_{1,j} = 0,\ j \geq R+3$. The symmetry of A yields:

$$A_k = A_{-k}. \tag{7.1}$$

Define $g(t) := b(e^{it}), \quad t \in (-\pi,\pi)$. Using (7.1), we obtain:

$$g(t) = A_{1,1} + 2\sum_{k=1}^{R+1} A_{1,(k+1)}\cos(tk). \tag{7.2}$$

Note that $g(0)$ is exactly the sum of a row corresponding to an interior node, hence, is zero as discussed in Section 5.1. In addition, $g'(0) = 0$. By using the fact that the off-diagonal entries are negative and the zero row sum property, we conclude that $g(t)$ is nonnegative. In addition, it has a unique root of order 2 at $t = 0$. Consequently, we obtain the following:

$$\begin{aligned} g(t) &= t^2\left(\frac{g''(0)}{2} + \mathcal{O}(t)\right) \\ &=: t^2 z(t). \end{aligned} \tag{7.3}$$

The following characterization of the minimal eigenvalue was given in [31]:

$$\lambda_{\min}(T_N(b)) \sim \frac{\pi^2}{N^2} z(0), \tag{7.4}$$

where $p_N \sim q_N$ means that $p_N/q_N \to 1$ as $N \to \infty$. See the discussion about the factor π^2 in [9, Eqn. (2) and (3)].

Using (7.3), we immediately see that $z(0) = \frac{g''(0)}{2}$. Therefore, it is imperative to obtain an explicit expression of $g''(0)$ using Table 5.1 for which the following formula holds:

$$g''(t) = -2\sum_{k=1}^{R+1} k^2 A_{1,(k+1)}\cos(tk). \tag{7.5}$$

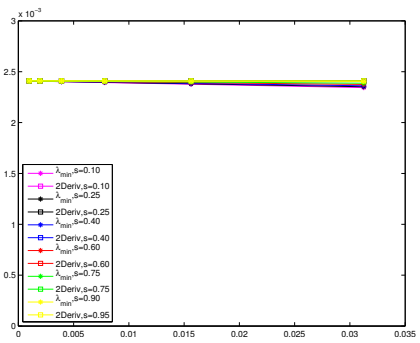

(a) $\lambda_{\min}$ and 2Deriv-bound vs δ. Fixed h.

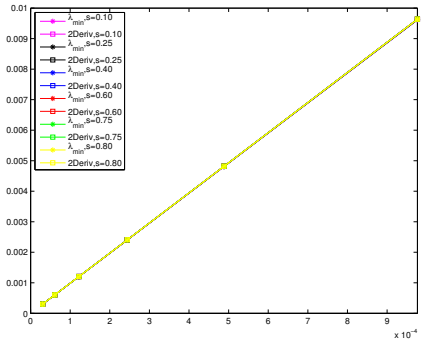

(b) $\lambda_{\min}$ and 2Deriv-bound vs h. Fixed δ.

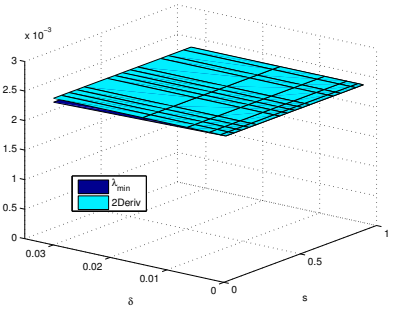

(c) $\lambda_{\min}$ and 2Deriv-bound vs δ and s. Fixed h.

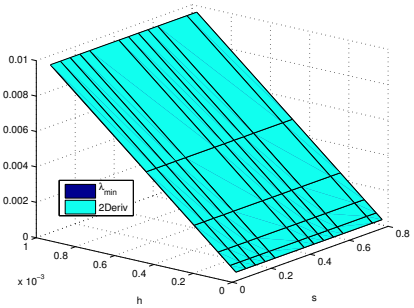

(d) $\lambda_{\min}$ and 2Deriv-bound vs h and s. Fixed δ.

FIG. 7.1. *Comparison of $\lambda_{\min}$ and the bound obtained by using the second derivative in (7.7), which we denote by 2Deriv-bound. Apparently 2Deriv-bound, which is $\pi^2 h$, is sharp. $h = 1/2^{12}$ and $\delta = 1/2^8$ are the fixed values.*

After some algebraic manipulation, we arrive at the remarkably simple result:

$$g''(0) = 2h^{-1}, \tag{7.6}$$

for linear finite elements. Combining (7.4) and (7.6), and letting $h = 1/N$, we obtain:

$$\lambda_{\min}(T_N(b)) \sim \pi^2 h. \tag{7.7}$$

(7.7) is in total agreement with the computed data of $\lambda_{\min}$ in Figure 7.1. Hence, (7.7) is numerically sharp. We further conclude that the constant $\underline{c}$ in (1.6) asymptotically behaves like π^2.

One may examine if a similar approach based on Toeplitz matrix properties used to determine the constant involved in $\lambda_{\min}$ quantification can be used for $\lambda_{\max}$. We motivate this avenue of study because there is an interesting relation of extremal eigenvalues of Toeplitz matrices. When one of them is available, the other can be potentially obtained using the following property [8]:

$$\lambda_{\max}(T_N(b)) = b^* - \lambda_{\min}(T_N(b^* - b)),$$

where $b^* := \max_{t\in(-\pi,\pi)} b(t)$.

Let $t_{\max}$ be the point at which b^* is attained, i.e., $b^* = b(t_{\max})$. Define $\hat{b}(t) = b^* - b(t)$ and $\hat{g}(t) := \hat{b}(e^{it})$. One can see that $\hat{b}(t)$ has a root of order 2 at $t = t_{\max}$ because $t = t_{\max}$ being a critical point implies $\hat{g}'(t_{\max}) = -g'(t_{\max}) = 0$.

Similar to (7.3), a perturbation expansion yields:

$$\begin{aligned}\hat{g}(t) &= (t - t_{\max})^2 \left(\frac{\hat{g}''(t_{\max})}{2} + \mathcal{O}((t - t_{\max})) \right) \\ &=: (t - t_{\max})^2 \hat{z}(t).\end{aligned}$$

Utilizing (7.4) for $T_N(\hat{b})$, we arrive at:

$$\lambda_{\max}(T_N(b)) - b^* \sim \frac{1}{2} g''(t_{\max}) \pi^2 h^2. \tag{7.8}$$

But the formula (7.8) requires that the following issues are addressed:

- One has to guarantee that the extremal value is attained at exactly one point $t_{\max} \in [0, \pi)$.
- One has to identify $t_{\max}$, hence, b^*.

Note that in the case of several extremal values, lower and upper asymptotic bounds for $\lambda_{\max}(T_N(b)) - b^*$ can be obtained from [8, Thm. 10.1].

The utilization of the symbol for identifying $\lambda_{\min}$ works conveniently because $g''(0)$ has no $\cos(tk)$ term which makes δ-, h-, and s-quantification in $\lambda_{\min}$ tractable. However, for $\lambda_{\max}$, $g''(t_{\max})$ with $t_{\max} \neq 0$ will involve the $\cos(tk)$ in (7.5). Even if the two issues above are addressed, (7.5) may potentially lead to intractable quantifications.

(a) piecewise linear

$A_{1,1}$	$\delta^{-1}\frac{4R-3}{R^2}$		≥ 0
$A_{1,2}$	$\delta^{-1}\frac{R-3}{R^2}$,	$R \geq 3$	≥ 0
$A_{1,j+1}$	$-\delta^{-1}\frac{3}{R^2}$,	$2 \leq j \leq R-2$	≤ 0
$A_{1,R}$	$-\delta^{-1}\frac{23}{8R^2}$		≤ 0
$A_{1,R+1}$	$-\delta^{-1}\frac{3}{2R^2}$		≤ 0
$A_{1,R+2}$	$-\delta^{-1}\frac{1}{8R^2}$		≤ 0

(b) piecewise constant

$A_{1,1}$	$3\delta^{-1}\frac{2R-1}{R^2}$		≥ 0
$A_{1,2}$	$-3\delta^{-1}\frac{1}{R^2}$,	$1 \leq j \leq R-1$	≤ 0
$A_{1,R+1}$	$-3\delta^{-1}\frac{1}{2R^2}$		≤ 0

TABLE 8.1

Stiffness matrix entries constructed by the corresponding finite element discretization for integrable kernel.

8. Integrable kernel. In this section, we analyze a closely related bilinear form $b(u, u)$ corresponding to the integrable kernel. The scaling factor in (2.2) implies:

$$c_\delta^{-1} := \frac{1}{\omega_d} \int_{B_\delta(0)} |x|^2 dx = \frac{\delta^{d+2}}{d+2}.$$

Then in 1D, $b(u, u)$ takes the following form:

$$b(u, u) = \frac{3}{2\delta^3} \int_{\overline{\Omega}} \int_{|x-y| \leq \delta} (u(x) - u(y))^2 dy dx.$$

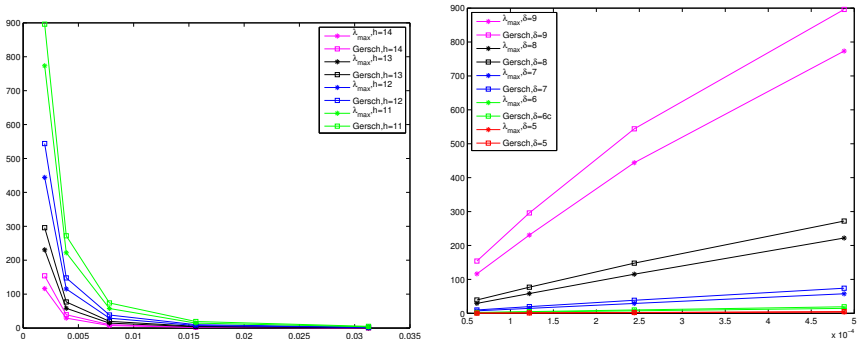

(a) $\lambda_{\max}$ and G-bound vs δ. Fixed h. (b) $\lambda_{\max}$ and G-bound vs h. Fixed δ.

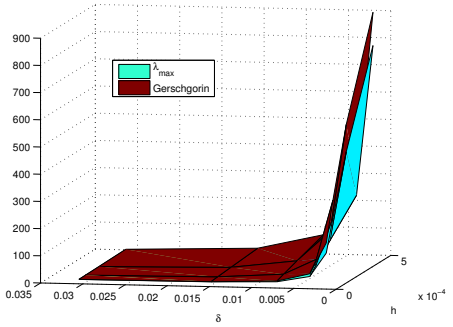

(c) $\lambda_{\max}$ and G-bound with respect to δ and h.

FIG. 8.1. *Comparison of* $\lambda_{\max}$ *and* G*-bound for integrable kernel.*

The first author had established the following spectral equivalence in [2, 3]:

$$\underline{\lambda} \leq \frac{b(u,u)}{\|u\|^2_{L^2(\overline{\Omega})}} \leq \overline{\lambda}^+ \delta^{-2},$$

which translates into the following eigenvalue estimate:

$$\underline{c} h^d \leq \lambda \leq \overline{c}^+ h^d \delta^{-2}, \tag{8.1}$$

where positive constants $\underline{c}$ and $\overline{c}^+$ are independent of h and δ. (8.1) is important in the sense that it implies that the condition number can be bounded independently from h. However, it turns out that (8.1) suppresses the exact h- and δ-quantifications. We can overcome this complication by resorting again to the Gerschgorin circle theorem and the same analysis based on matrix entries as we did for the singular kernel case. There is an interesting difference in the sign of the $A_{1,2}$ entry for the case of linear finite elements. Namely, when $R \geq 3$, $A_{1,2}$ becomes positive as opposed to the singular kernel case. Thus, utilizing the zero row sum property, the Gerschgorin bound takes the form:

$$\lambda \leq 2(A_{1,1} + A_{1,2}). \tag{8.2}$$

From Table 8.1, we see that the δ- and h-quantifications of $A_{1,1}$ and $A_{1,2}$ are exactly the same:

$$\begin{aligned} A_{1,1} + A_{1,2} &= \delta^{-1} \frac{5R - 6}{R^2} \\ &= 5h\delta^{-2} - 6h^2\delta^{-3}. \end{aligned} \tag{8.3}$$

Combining (8.2) and (8.3), we eventually obtain:

$$\lambda_{\max} = \overline{c}(5h\delta^{-2} - 6h^2\delta^{-3}). \tag{8.4}$$

Furthermore, (8.2) is numerically sharp as demonstrated in Figure 8.1. We can also establish the sharpness (up to a constant) of h- and δ-quantifications in (8.4) by using a similar Rayleigh quotient argument as in the proof of (6.5) by simply choosing $\underline{u} = e_1 + e_2$ as in the proof of Lemma 6.2.

Note that (8.2) and (8.3) lead to the same upper bound we obtain from (8.1), if we drop the negative term $-6h^2\delta^{-3}$:

$$\lambda_{\max} \leq \overline{c}^{+} h\delta^{-2}.$$

Consequently, (8.4) completely reveals the exact h- and δ-quantifications. Combining (8.4) and (3.7), we find that the sharp condition number bound is as follows:

$$\kappa(A) \leq c(5\delta^{-2} - 6h\delta^{-3}). \tag{8.5}$$

Reflecting on what is available in the literature, we compare (8.5) with the bound given in [55, p. 1772]:

$$\kappa(A) \leq c \min\{\delta^{-2}, h^{-2}\}. \tag{8.6}$$

In the important nonlocal regime (6.9), (8.6) defaults to our estimate (8.1) obtained by dropping the negative term in (8.4).

Furthermore, in the regime of (6.9), we see that the $5\delta^{-2}$ term is dominant over $6h\delta^{-3}$. Hence, the condition number behaves like δ^{-2} and the power of h in the non-dominant term is only 1, (neither -2 nor -3), implying that the growth of the condition number with respect to h is less pronounced. Hence, the condition number weakly depends on h. This is in agreement with our 1D numerical experiments previously reported in [3, Table 4.1 and Fig. 4.1.a]. Also see the similar result for 2D numerical experiments [3, Table 4.2 and Fig. 4.2.a].

The same δ- and h-quantification (up to a constant) of $\lambda_{\max}$ in (8.3) obtained using piecewise linear discretization holds for the piecewise constant case; see $A_{1,1}$ entry in Table 8.1 and note that this time $A_{1,2}$ entry is negative.

9. Conclusion. The main goal of this article was to construct sharp quantifications of $\lambda_{\min}$ and $\lambda_{\max}$ in all three parameters δ, h, and s in 1D. We accomplished sharpness both rigorously and numerically. We identified the behaviour of the condition number as follows: It gets larger as $\delta \to 0$ (as the operator approaches to its corresponding local analog) and it becomes largest as $s \to 1$ (when the singularity is at its worst); see Figure 9.1(a). The condition number with respect to h is moderate for almost all values of h. However, as $s \to 1$ and $h \to 0$ the condition number blows up; see Figure 9.1(b).

We studied the scaled operator (1.2) because it provided direct analogy to the local operator. The scaling (2.2) prevented degeneracy of (1.2) as $\delta \to 0$. Furthermore,

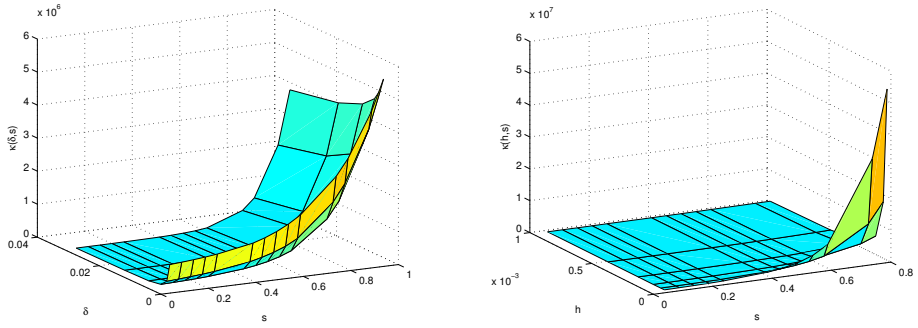

(a) Vary δ, fixed h; $h = 1/2^{12}$. (b) Vary h, fixed δ; $\delta = 1/2^{8}$.

FIG. 9.1. *Condition number for singular kernel with piecewise linear finite element discretization.*

the scaling conveniently caused $\lambda_{\min}$ to depend only on h. Hence, the δ- and s-quantifications of the condition number reduced to that of $\lambda_{\max}$.

We established the quantification of $\lambda_{\min}$ by nonlocal characterization of Sobolev spaces. The quantification of $\lambda_{\max}$, on the other hand, was established by connecting the bilinear form to H^1 and H^s by using norm estimates; see (4.1) and (4.5), respectively. (4.1) and (4.5) revealed both δ and s dependence. Subsequently, the explicit bound of $\lambda_{\max}$ was obtained using inverse estimates. The utilized functional analysis tools are strong in the sense that the results are valid for any dimension. However, they are weak in the sense that they obscure dependence on parameters. The inverse estimate constant depends on the order of finite element, shape regularity of mesh, and s. The parameter s plays a crucial role in our analysis. Identifying the s-quantification was important especially for limiting s values, $s \to 0$ and $s \to 1$, and we observed blowup in the estimates occur near $s = 1$.

Revealing δ-, h-, and s-quantifications require analysis which is more sensitive. Working directly with the matrix entries was necessary for such a task. By resorting to explicit linear algebra, we assembled the stiffness matrix by systematically identifying its entries through a nontrivial computation which involved 8 iterated integrals; see (5.5). Introducing a new parameter, the ratio $R = \frac{\delta}{h}$, dramatically simplified the involved algebra. It was also remarkable that the second derivative of the symbol $g(t)$ in (7.2) evaluated at 0 turned out to be $2h^{-1}$; see (7.6).

We employed two different algebraic approaches for $\lambda_{\max}$ and $\lambda_{\min}$. The negativity of off-diagonal entries with zero row sum property provided significant advantage for establishing an upper bound of $\lambda_{\max}$ through the use of the Gerschgorin circle theorem. Amazingly, the Gerschgorin-bound captured sharp quantifications with respect to all three parameters up to a constant; see (6.5). The Gerschgorin technique heavily depends on identifying the matrix entries. Therefore, it might be difficult to obtain the matrix entries especially in 3D because each of them involves 6 dimensional integrals and this is a major limitation of the matrix entry approach. On the other hand, for $\lambda_{\min}$, we exploited the Toeplitz property of the stiffness matrix. There is substantial literature on the extremal eigenvalues of banded Toeplitz matrices. Using related results, we verified the result obtained by nonlocal characterization of Sobolev spaces, $\lambda_{\min} = ch$, and were even able to exactly identify the involved constant, $\underline{c}$ scaled like π^2 as $h \to 0$.

The first author had studied the integrable kernel case [2, 3]. Using the above algebraic techniques, we improved (8.1) and fully revealed the missing h-quantification. As a side result, we established that these techniques also give exactly the same sharp quantifications for a simpler discretization such as piecewise constant finite elements.

Consequently, the results obtained through algebraic techniques hold only for 1D. For higher dimensions, we plan to investigate further algebraic techniques utilizing the matrix structure for future research. There is substantial numerical evidence from the first author's article [3] indicating that the 2D results for the integrable kernel case are in agreement with the 1D results. Hence, our 1D results can potentially be generalized to higher dimensions.

Acknowledgement. The authors would like to thank Albrecht Böttcher of Technische Universität Chemnitz for his kind advice concerning Toeplitz matrices. The first author would like to thank Michael L. Parks of Sandia National Labs for his encouragement and initiation of this avenue of research of nonlocal problems.

REFERENCES

[1] H. G. Aksoy and E. Senocak, *Discontinuous Galerkin method based on peridynamic theory for linear elasticity*, Int. J. Numer. Methods Engrg, 88 (2011), pp. 673–692.
[2] B. Aksoylu and T. Mengesha, *Results on nonlocal boundary value problems*, Numerical Functional Analysis and Optimization, 31 (2010), pp. 1301–1317.
[3] B. Aksoylu and M. L. Parks, *Variational theory and domain decomposition for nonlocal problems*, Applied Mathematics and Computation, 217 (2011), pp. 6498–6515.
[4] B. Alali and R. Lipton, *Multiscale dynamics of heterogeneous media in the peridynamic formulation*, Journal of Elasticity, 106 (2012), pp. 71–103.
[5] F. Andreu-Vaillo, J. M. Mazon, J. D. Rossi, and J. Toledo-Melero, *Nonlocal Diffusion Problems*, vol. 165 of Mathematical Surveys and Monographs, American Mathematical Society and Real Socied Matematica Espanola, 2010.
[6] E. Askari, F. Bobaru, R. B. Lehoucq, M. L. Parks, S. A. Silling, and O. Weckner, *Peridynamics for multiscale materials modeling*, Journal of Physics: Conference Series, 125 (2008), p. (012078). SciDAC 2008, Seattle, Washington, July 13-17, 2008.
[7] G. Aubert and P. Kornprobst, *Can the nonlocal characterization of Sobolev spaces by Bourgain et al. be useful for solving variational problems?*, SIAM J. Numer. Anal., 47 (2009), pp. 844–860.
[8] A. Böttcher and S. M. Grudsky, *Spectral properties of banded Toeplitz matrices*, SIAM, 2005.
[9] A. Böttcher and H. Widom, *From Toeplitz Eigenvalues through Green's Kernels to Higher-order Wirtinger-Sobolev Inequalities*, Operator Theory: Advances and Applications, 171 (2007), pp. 73–87.
[10] J. Bourgain, H. Brézis, and P. Mironescu, *Another look at Sobolev spaces*, In: J.L. Menaldi, E. Rofman and A. Sulem, Editors, Optimal Control and Partial Differential Equations,, A volume in honour of A. Benssoussan's 60th birthday (2001), pp. 439–455.
[11] E. Celik, I. Guven, and E. Madenci, *Simulations of nanowire bend tests for extracting mechanical properties*, Theoretical and Applied Fracture Mechanics, 55 (2011), pp. 185–191.
[12] X. Chen and M. Gunzburger, *Continuous and discontinuous finite element methods for a peridynamics model of mechanics*, Comput. Methods Appl. Mech. Engrg, 200 (2011), pp. 1237–1250.
[13] E. Di Nezza, G. Palatucci, and E. Valdinoci, *Hitchhiker's guide to fractional Sobolev spaces*, Bull. Sci. math., 136 (2012), pp. 521–573.
[14] Q. Du, M. Gunzburger, R. B. Lehoucq, and K. Zhou, *Analysis and approximation of nonlocal diffusion problems with volume constraints*, SIAM Rev., 54 (2012), pp. 667–696.
[15] ———, *Analysis of the volume-constrained peridynamic Navier equation of linear elasticity*, J. Elast., 113 (2013), pp. 193–217.
[16] ———, *A nonlocal vector calculus, nonlocal volume-constrained problems, and nonlocal balance laws*, Math. Mod. Meth. Appl. Sci., 23 (2013), pp. 493–540.

[17] Q. Du, L. Ju, L. Tian, and K. Zhou, *A posteriori error analysis of finite element method for linear nonlocal diffusion and peridynamic models*, Math. Comp., (2013), pp. 1889–1922.
[18] Q. Du, J. R. Kamm, R. B. Lehoucq, and M. L. Parks, *A new approach for a nonlocal, nonlinear conservation law*, SIAM Journal on Applied Mathematics, 72 (2012), pp. 464–487.
[19] Q. Du, L. Tian, and X. Zhao, *A convergent adaptive finite element algorithm for nonlocal diffusion and peridynamic models.* to appear in SIAM J. Numer. Anal., 2013.
[20] Q. Du and K. Zhou, *Mathematical analysis for the peridynamic nonlocal continuum theory*, ESAIM: Mathematical Modelling and Numerical Analysis, 45 (2011), pp. 217–234.
[21] N. Duruk, H. A. Erbay, and A. Erkip, *A higher-order Boussinesq equation in locally nonlinear theory of one-dimensional non-local elasticity*, IMA Journal of Applied Mathematics, 74 (2009), pp. 97–106.
[22] ———, *Global existence and blow-up for a class of nonlocal nonlinear Cauchy problems arising in elasticity*, Nonlinearity, 23 (2010), pp. 107–118.
[23] ———, *Blow-up and global existence for a general class of nonlocal nonlinear coupled wave equations*, J. Differential Equations, (2011), pp. 1448–1459.
[24] E. Emmrich, R. B. Lehoucq, and D. Puhst, *Peridynamics: a nonlocal continuum theory*, in Meshfree Methods for Partial Differential Equations VI, M. Griebel and M. A. Schweitzer, eds., vol. 89, Springer, 2013, pp. 45–65.
[25] E. Emmrich and O. Weckner, *On the well-posedness of the linear peridynamic model and its convergence towards the Navier equation of linear elasticity*, Commun. Math. Sci., 5 (2007), pp. 851–864.
[26] ———, *The peridynamic equation and its spatial discretization*, Math. Model. Anal., 12 (2007), pp. 17–27.
[27] G. Gilboa and S. Osher, *Nonlocal operators with applications to image processing*, Multiscale Modeling and Simulation, 7 (2008), pp. 1005–1028.
[28] M. D. Gunzburger and R. B. Lehoucq, *A nonlocal vector calculus with application to nonlocal boundary value problems*, Multiscale Model. Simul., 8 (2010), pp. 1581–1598.
[29] D. Hertz, *Simple Bounds on the Extreme Eigenvalues of Toeplitz Matrices*, IEEE Transactions on Information Theory, 38 (1992), pp. 175–176.
[30] B. Hinds and P. Radu, *Dirichlet's principle and wellposedness of steady state solutions for a nonlocal peridynamics model*, Applied Mathematics and Computation, 219 (2012), pp. 1411–1419.
[31] M. Kac, W. L. Murdock, and G. Szegö, *On the eigenvalues of certain hermitian forms*, J. Rational Mech. Anal., 2 (1953), pp. 767–800.
[32] B. Kilic, A. Agwai, and E. Madenci, *Peridynamic theory for progressive damage prediction in centre-cracked composite laminates*, Composite Structures, 90 (2009), pp. 141–151.
[33] B. Kilic and E. Madenci, *Prediction of crack paths in a quenched glass plate by using peridynamic theory*, Int. J. Fract., 156 (2009), pp. 165–177.
[34] ———, *Coupling of peridynamic theory and finite element method*, Journal of Mechanics of Materials and Structures, 5 (2010), pp. 707–733.
[35] R. Lehoucq and S. Silling, *Convergence of peridynamics to classical elasticity*, J. Elast., 93 (2008), pp. 13–37. doi:10.1007/s10659-008-9163-3.
[36] ———, *Force flux and the peridynamic stress tensor*, J. Mech. Phys. Solids, 56 (2008), pp. 1566–1577.
[37] R. B. Lehoucq and S. Silling, *Peridynamic theory of solid mechanics*, Advances in Applied Mechanics, 44 (2010), pp. 73–168.
[38] E. Madenci and E. Oterkus, *Peridynamic Theory and Its Applications*, Springer, 2014.
[39] T. Mengesha, *Nonlocal Korn-type characterization of Sobolev vector fields*, Communication in Comtemporary Mathematics, 14 (2012), pp. 1250028, (28 pp.).
[40] T. Mengesha and Q. Du, *Analysis of a scalar peridynamic model for sign changing kernel*, Disc. Cont. Dyn. Sys. B, 18 (2013), pp. 1415–1437.
[41] Y. Mikata, *Analytical solutions of peristatic and peridynamics problems for a 1D infinite rod*, International Journal of Solids and Structures, 49 (2012), pp. 2887–2897.
[42] E. Oterkus and E. Madenci, *Peridynamic analysis of fiber reinforced composite materials*, Journal of Mechanics of Materials and Structures, 7 (2012), pp. 45–84.
[43] ———, *Peridynamic theory for damage initiation and growth in composite laminate*, Key Engineering Materials, 488–489 (2012), pp. 355–358.
[44] E. Oterkus, E. Madenci, O. Weckner, S. S. Silling, P. Bogert, and A. Tessler, *Combined finite element and peridynamic analyses for predicting failure in a stiffened composite curved panel with a central slot*, Composite Structures, 94 (2012), pp. 839–850.
[45] A. C. Ponce, *An estimate in the spirit of Poincare's inequality*, J. Eur. Math. Soc., 6 (2004),

pp. 1–15.
[46] P. Seleson, S. Beneddine, and S. Prudhomme, *A force-based coupling scheme for peridynamics and classical elasticity*, Computational Materials Science, 66 (2013), pp. 34–49.
[47] P. Seleson, M. Gunzburger, and M. L. Parks, *Interface problems in nonlocal diffusion and sharp transitions between local and nonlocal domains*, Computer Methods in Applied Mechanics and Engineering, (2013). In press.
[48] ———, *Peridynamic state-based models and the embedded-atom model*, Communications in Computational Physics, 15 (2014), pp. 179–205.
[49] P. Seleson and M. L. Parks, *On the role of the influence function in the peridynamic theory*, International Journal for Multiscale Computational Engineering, 9 (2011), pp. 689–706.
[50] P. Seleson, M. L. Parks, M. Gunzburger, and R. B. Lehoucq, *Peridynamics as an upscaling of molecular dynamics*, Multiscale Model. Simul., 8 (2009), pp. 204–227.
[51] S. Silling, *Reformulation of elasticity theory for discontinuities and long-range forces*, J. Mech. Phys. Solids, 48 (2000), pp. 175–209.
[52] S. A. Silling and F. Bobaru, *Peridynamic 3D problems of nanofiber networks and carbon nanotube-reinforced composites*, in Materials and Design: Proc. Numiform, American Institute of Physics, 2004, pp. 1565–1570.
[53] ———, *Peridynamic modeling of membranes and fibers*, Int. J. Nonlinear Mech., 40 (2005), pp. 395–409.
[54] X. Tian and Q. Du, *Analysis and comparison of different approximations to nonlocal diffusion and linear peridynamic equations*, SIAM J. Numer. Anal., (2013). To appear.
[55] K. Zhou and Q. Du, *Mathematical and numerical analysis of linear peridynamic models with nonlocal boundary conditions*, SIAM J. Numer. Anal., 48 (2010), pp. 1759–1780.